Emissions from the laboratory combustion of wildland fuels: Particle morphology and size

Rajan K. Chakrabarty,[1] Hans Moosmüller,[1] Mark A. Garro,[1,2] W. Patrick Arnott,[1,3] John Walker,[1,4] Ronald A. Susott,[5] Ronald E. Babbitt,[5] Cyle E. Wold,[6] Emily N. Lincoln,[6] and Wei Min Hao[6]

Received 9 September 2005; revised 30 November 2005; accepted 6 January 2006; published 5 April 2006.

[1] The morphology of particles emitted by wildland fires contributes to their physical and chemical properties but is rarely determined. As part of a study at the USFS Fire Sciences Laboratory (FSL) investigating properties of particulate matter emitted by fires, we studied the size, morphology, and microstructure of particles emitted from the combustion of eight different wildland fuels (i.e., sagebrush, poplar wood, ponderosa pine wood, ponderosa pine needles, white pine needles, tundra cores, and two grasses) by scanning electron microscopy. Six of these fuels were dry, while two fuels, namely the tundra cores and one of the grasses, had high fuel moisture content. The particle images were analyzed for their density and textural fractal dimensions, their monomer and agglomerate number size distributions, and three different shape descriptors, namely aspect ratio, root form factor, and roundness. The particles were also probed with energy dispersive X-ray spectroscopy confirming their carbonaceous nature. The density fractal dimension of the agglomerates was determined using two different techniques, one taking into account the three-dimensional nature of the particles, yielding values between 1.67 and 1.83, the other taking into account only the two-dimensional orientation, yielding values between 1.68 and 1.74. The textural fractal dimension that describes the roughness of the boundary of the two-dimensional projection of the particle was between 1.10 and 1.19. The maximum length of agglomerates was proportional to a power a of their diameter and the proportionality constant and the three shape descriptors were parameterized as function of the exponent a.

Citation: Chakrabarty, R. K., H. Moosmüller, M. A. Garro, W. P. Arnott, J. Walker, R. A. Susott, R. E. Babbitt, C. E. Wold, E. N. Lincoln, and W. M. Hao (2006), Emissions from the laboratory combustion of wildland fuels: Particle morphology and size, *J. Geophys. Res.*, *111*, D07204, doi:10.1029/2005JD006659.

1. Introduction

[2] Particulate matter (PM) in the atmosphere influences the Earth's radiation balance and climate [*Haywood and Ramaswamy*, 1998; *National Research Council*, 1996], atmospheric chemistry [*Finlayson-Pitts and Pitts*, 2000], visibility [*National Research Council*, 1993; *Watson*, 2002], and the health of living beings including humans [*National Research Council Committee on Research Priorities for Airborne Particulate Matter*, 1998; *Vedal*, 1997] on scales ranging from local to global. On a global scale, direct radiative effects from PM of directly anthropogenic origin (as opposed to dust entrainment caused by desertification) are dominated by sulfate and carbonaceous PM [*Schult et al.*, 1997]. While sulfate PM has a very high albedo and predominantly scatters light in the visible part of the spectrum, carbonaceous PM contains components that both scatter and absorb visible light resulting in a wide range of albedos [*Horvath*, 1993]. The strongly light absorbing component is called black carbon (BC), while the mostly scattering component is called organic carbon (OC). BC and OC can coexist in internally mixed particles that may consist of a BC core coated with OC. In addition to the direct radiative effects of carbonaceous PM [*Haywood and Ramaswamy*, 1998], it can also serve as cloud condensation nuclei (indirect effect) [*Novakov and Penner*, 1993] and assist with the evaporation of clouds due to light absorption and heating by BC (semi-direct effect) [*Ackerman et al.*, 2000; *Lohmann and Feichter*, 2001]. Transport, deposition, chemistry, radiative effects, and health effects of PM depend largely on its composition, size distribution, morphology, and shape [*Seinfeld and Pandis*, 1998].

[1]Desert Research Institute, Nevada System of Higher Education, Reno, Nevada, USA.
[2]Now at Department of Chemistry, Harvard University, Cambridge, Massachusetts, USA.
[3]Now at Department of Physics, University of Nevada, Reno, Nevada, USA.
[4]Now at Droplet Medical Technologies, Boulder, Colorado, USA.
[5]Retired from USDA Forest Service, Rocky Mountain Research Station, Fire Sciences Laboratory, Missoula, Montana, USA.
[6]USDA Forest Service, Rocky Mountain Research Station, Fire Sciences Laboratory, Missoula, Montana, USA.

Copyright 2006 by the American Geophysical Union.
0148-0227/06/2005JD006659$09.00

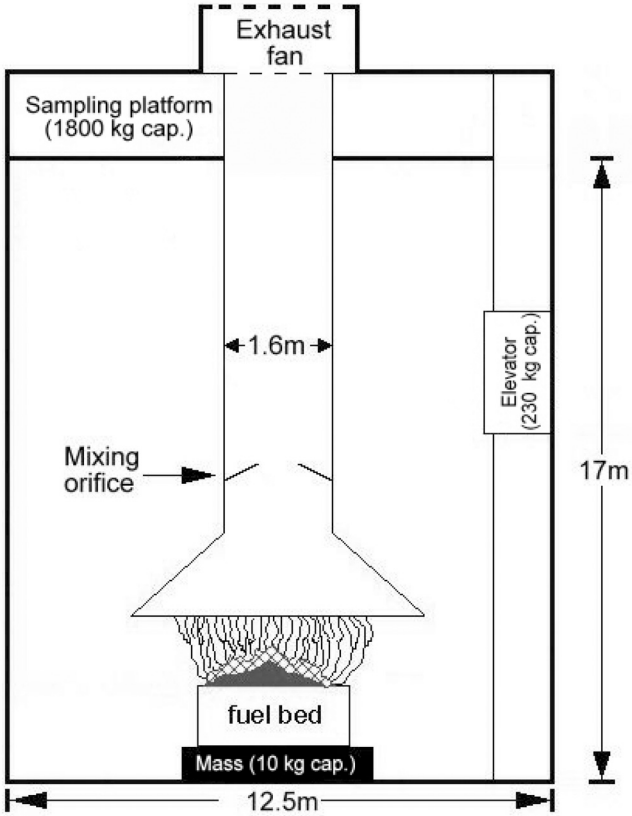

Figure 1. Schematic diagram of the FSL combustion facility [*Christian et al.*, 2003].

[3] Wildland fires of both anthropogenic and natural origin are a major source of carbonaceous PM in the global atmosphere [*Kasischke and Penner*, 2004; *Seiler and Crutzen*, 1980]. The properties of PM emitted by wildland fires vary strongly and are largely determined by fuel properties and combustion conditions [*Reid et al.*, 2005]. Combustion conditions are often classified by a combination of two combustion phases. High-temperature flaming combustion produces black PM, often consisting of fractal chain aggregates, that has a high BC content, low albedo, and therefore strongly absorbs visible light. Low-temperature smoldering combustion, on the other hand, produces white PM, often consisting of near-spherical particles, that has a high OC content, high albedo, and therefore predominantly scatters visible light. The physical characteristics of carbonaceous aerosol particles are determined by a combination of their morphology, monomer size, and shape [*Martins et al.*, 1998b; *Pósfai et al.*, 2003; *Reid and Hobbs*, 1998]. Unfortunately, very little is known about the morphology, size distribution, and shape of particles emitted from the combustion of wildland fuels.

[4] Previous studies have shown PM from biomass burning to occur as a mixture of spherical and nonspherical particles and chain agglomerates [*Martins et al.*, 1998b]. These studies sampled emissions from the combustion of mixed wildland fuels at forest fire sites in North and South America. In contrast, our work studies the morphology, size, and shape of PM freshly emitted from the combustion of individual wildland fuels under controlled laboratory conditions. An extensive series of measurements was performed during a 2-week measurement period that took place during November 2003 in the Combustion Laboratory of the Missoula Fire Science Laboratory (FSL). The purpose of this study was to improve our understanding of the optical properties of particles emitted by wildland fires [*Chen et al.*, 2006; *Rinehart et al.*, 2005]. Scanning electron microscopy (SEM) was used to provide a direct observation of the morphology, monomer size, and shape of the PM emitted by the combustion of different fuels. Energy-dispersive X-ray analysis was performed to confirm the carbonaceous nature of the PM. SEM images of PM were analyzed using the concept of fractal dimension, which has found widespread use in the field of aerosol science, especially when it comes to morphological quantification of agglomerated aerosols and their optical properties [*Colbeck and Nyeki*, 1992; *Kindratenko et al.*, 1994; *Sorensen*, 2001]. A measurement of the 2-D (two-dimensional) and 3-D (three-dimensional) density fractal dimension and 2-D texture fractal dimension was performed on the agglomerated aerosol particles using computer-aided image analysis. The shape of the particles was characterized using three conventional shape descriptors [*Hentschel and Page*, 2003] aspect ratio, circularity (both sensitive to elongation), and root form factor (sensitive to boundary irregularity).

[5] The experimental and analytical methods are described in section 3. Results from the analysis of SEM images of particles from the combustion of different fuels are presented in section 4. A summary of the results and suggestions for future work are provided in section 5.

2. Experimental

2.1. Fuel and Fire Preparation

[6] The combustion facility at FSL measures 12.5 m by 12.5 m by 22 m high (Figure 1) [*Christian et al.*, 2003]. A 1.6-m diameter exhaust stack with a 3.6 m inverted funnel opening extends from 2 m above the floor through the ceiling. The room is pressurized with outside air that has been conditioned for temperature and humidity and is then vented through the stack, completely entraining the emissions from fires burning beneath the funnel. The fires are burned on a continuously weighed fuel bed. Fuels and ashes from each burn are collected for analysis yielding carbon (C), nitrogen (N), ash, and fuel moisture (FM) content as fraction of dry mass (Table 1). Fuel moisture was determined by measuring the mass loss after holding the sample at 90°C overnight. Eight different wildland fuels (see Table 1), namely sagebrush, poplar wood, ponderosa pine wood, ponderosa pine needles, white pine needles, tundra cores, dambo grass, and Montana grass (i.e., freshly cut grass from outside of the laboratory) were used for a total of 70 burns. Six fuels were "dry" from long-term indoor storage with a fuel moisture content ranging from 5 to 10% of dry mass, while Montana grass and the tundra cores were "wet" with a substantially higher fuel moisture content on the order of 20% for Montana grass. Fuels were prepared for combustion by arranging them in a round "pie" shape and ignited in the center of the "pie".

[7] A sampling platform surrounds the stack at 17 m elevation where all the temperature, pressure, gas, and

Table 1. Fuel Information With Carbon (C), Nitrogen (N), Ash, and Fuel Moisture (FM) Content Given as Fraction of Dry Mass

Fuel Name	Fuel Description	Origin	C, %	N, %	Ash, %	FM,[b] %	Fuel Mass,[a] g
Sagebrush	Sagebrush	US	48	0.92	3.5	8.3 ± 1.9	250
Poplar Wood	Excelsior (Shredded Aspen Wood Product)	US	48	0.07	0.64	5.9 ± 0.5	250
Ponderosa Pine Wood	Ponderosa Pine Wood Sticks	US	49	0.07	0.28	6.0 ± 0.4	250
Ponderosa Pine Needles	Ponderosa Pine Needles	US	50	0.6	3.8	7.3 ± 0.8	250
White Pine Needles	White Pine Needles	US	49	0.50	4.3	8.2 ± 0.7	250
Montana Grass	Fresh Montana Grass	US	44	0.17	4.2	17.5	250
Dambo Grass	Dry Land Dambo Grass	Zambia	45	0.34	4.3	6.3 ± 0.5	250
Tundra Core	Wet Tundra Core	Alaska	NA	NA	NA	113 ± 126	1250

[a]Fuel mass is the nominal fuel mass used for each burn.
[b]Fuel Moisture (FM) ranges are given as standard deviation, no errors are given for Montana Grass as only two measurements (FM = 18.3% and FM = 16.8%) were made. The large variability for the Tundra Core is in part due to the large inhomogeneity of the core.

particle measurement and sampling equipment for this experiment was deployed. Sampling pumps were deployed on the ground floor with long, flexible pipes connecting them to the equipment on the measurement platform. Additional equipment on the ground floor included cameras for continuous visible and infrared imagery of the combustion process.

2.2. Scanning Electron Microscopy (SEM) Analysis

[8] For SEM analysis, aerosol samples were collected on the 17-m elevation, sampling platform by drawing a sample from the center of the smoke stack. Particles were sampled on Nuclepore clear polycarbonate 13-mm diameter filters mounted in Costar Pop-Top Membrane holders. After sampling, the filter samples were kept in refrigerated storage and later prepared for SEM analysis by coating them with a 1-nm thick layer of platinum to prevent aerosol charging during SEM analysis. The coated filters were analyzed using a Hitachi Scanning Electron Microscope Model S-4700 at the Metallurgical and Materials Engineering Department of the University of Nevada, Reno. Images of around 300–400 particles were selected for each fuel type and analyzed for particle shape, fractal dimension, agglomerate size distribution, and monomer size distribution. The selection of particles was based on the random distribution of particles on the SEM filter.

[9] SEM analysis may change the shape of particles through heat damage and physical damage. Heat damage evaporates semivolatile components from the filter due to the high accelerating voltage of the electron beam (e.g., 10–20 kV) operating under vacuum conditions. Physical damage distorts the original particle shape because of particle charging by the electron beam. Therefore only nonvolatile particle components could be characterized with the SEM. The influence of the accelerating voltage of the electron beam on the shape on the aerosol particles was characterized by varying the accelerating voltages between 10 and 25 kV. Within this voltage range, no or very little change in the shape of the aggregates was observed. In this study a relatively moderate accelerating voltage of 20 kV was used for most images. Compared to lower accelerating voltages, the use of 20 kV improves imaging of the surface and internal structure of the particles. At this operating voltage, shape distortion due to charging was observed in less than 3% of the aggregates.

2.3. Fractal Analysis

[10] Since the introduction of the concept of fractal dimension by *Mandelbrot* [1982], it has found significant use in atmospheric sciences, especially in describing the complex structures resulting from random aggregation of fine aerosol particles. These structures are difficult to describe using regular Euclidean geometry. In 3-D, the number N of fine particles aggregating to make up a cluster with fractal morphology scales with the radius of gyration R_g as [*Mandelbrot*, 1982]

$$N = k_g \left(\frac{2R_g}{d_p} \right)^{D_f}, \tag{1}$$

where k_g is the fractal proportionality constant, d_p is the primary particle diameter, and D_f is the mass fractal dimension. For a given radius of gyration, the higher the fractal dimension, the higher is the number of primary particles in agglomerate, thus resulting in a higher number or mass density. Fractal dimensions can be calculated based on the perimeter or the density. The density fractal dimension describes the space-filling characteristics of the aggregate [*Katrinak et al.*, 1993]. The 2-D density fractal dimension can be calculated using image-processing algorithms from a 2-D image of agglomerate and it is often used as approximation of the 3-D density fractal dimension D_f (equation (1)). The textural fractal dimension is useful for describing the 2-D texture of the agglomerate [*Kaye*, 1989]. The value of the textural fractal dimension should approach two as particles become smoother (more circular). Past studies have shown that aerosol aggregates with chain-like structures, formed by collisions of smaller chains, usually have density fractal dimension between 1.5 and 1.9 and textural fractal dimension between 1.05 and 1.4 [*McDonald and Biswas*, 2004].

[11] Particle images were analyzed for the density fractal dimension and the textural fractal dimension using image analysis software for the determination of the density fractal dimension (i.e., Digital Micrograph 3, Gatan Inc.) and the 2-D textural fractal dimension (i.e., ImageJ (Image Processing and Analysis in Java), National Institute of Health). The methodology used for calculating the density fractal dimensions of the particles is explained in detail in section 4.2b.

[12] The 2-D density fractal dimension was measured using the nested-square method [*Dye et al.*, 2000]. A

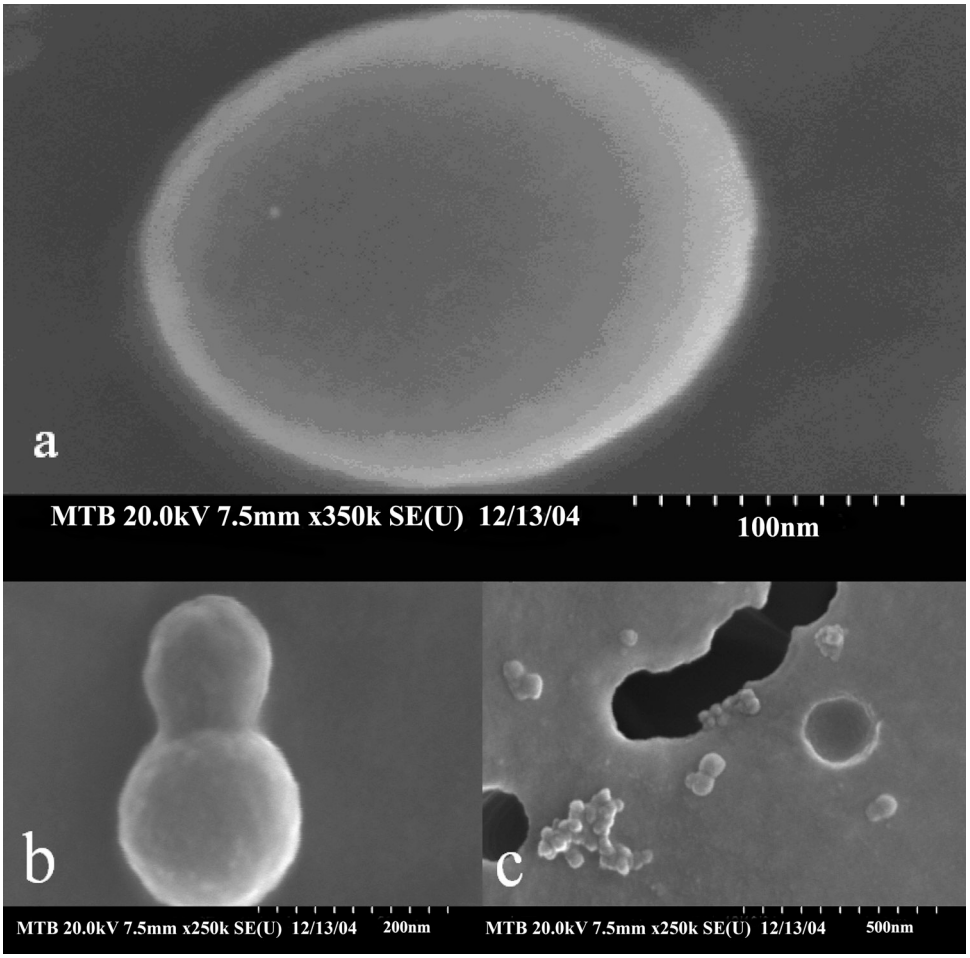

Figure 2. SEM images of tar balls from the combustion of Montana grass and tundra cores. These tar balls occur as (a) individual spherical particles as well as in (b) small and (c) large clusters.

customized macro available with ImageJ was used for implementing this algorithm. The macro first threshes the image to be analyzed. Threshing is a procedure that converts the image into a black and white image, where black pixels represent part of the particle and white represents everything else (not part of the agglomerate). The fractal dimension of the black and white digitized image is determined by covering the image with boxes (squares) and then evaluating how many boxes are needed to cover the agglomerate completely. This process is repeated several times, generating a list of box sizes and the number of boxes that contain part of the particle perimeter. The slope of the linear regression of the logarithm of the box size versus the logarithm of the number of boxes is the 2-D density fractal dimension.

[13] To calculate the 2-D textural fractal dimension, instead of evaluating how many boxes are needed to cover the agglomerate completely, the number of boxes through which the perimeter passes is evaluated.

2.4. Shape Analysis

[14] Although particle shape is an inherently three-dimensional attribute, many characterization techniques utilize two-dimensional data [*Stachowiak and Podsiadlo*, 2001]. So-called "conventional shape descriptors" combine two measures of particle size as a ratio [*Hentschel and Page*, 2003]. Because particle size can be defined in many different ways, a correspondingly large number of conventional shape descriptors exist. Each descriptor is most sensitive to a specific attribute of shape, depending upon the size measures selected. If more than two measures are available, the question arises as to which combination provides the best description of shape. On the basis of the findings by *Hentschel and Page* [2003], three simple shape descriptors were selected for our analysis, that is aspect ratio *AR*, root form factor *RFF*, and roundness *RN*. These shape descriptors can be calculated from the maximum projected width $W_{\max}$, maximum projected length $L_{\max}$, projected area A_a, and perimeter length P of the individual aggregates as

$$AR = \frac{W_{\max}}{L_{\max}}, \tag{2a}$$

$$RFF = \frac{\sqrt{4\pi A_a}}{P}, \text{ and} \tag{2b}$$

$$RN = \frac{4A_a}{\pi L_{\max}^2} \tag{2c}$$

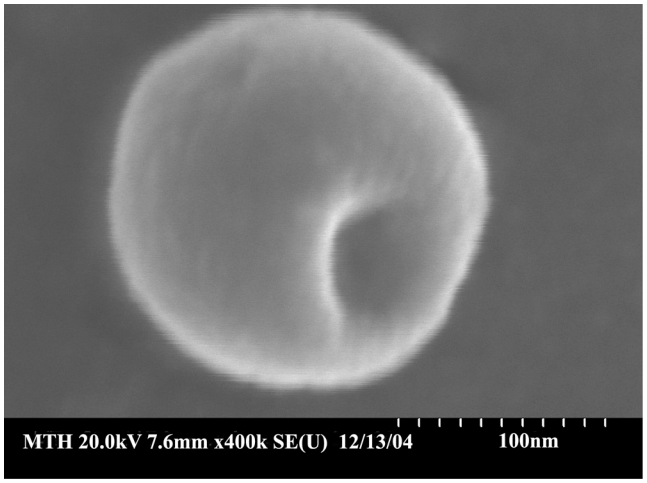

Figure 3. SEM image of a particle from the combustion of Montana grass showing structural defects sometimes found in spherical tar balls originating from the combustion of wet fuels.

Among these three shape descriptors, aspect ratio and roundness are sensitive to elongation, while root form factor is sensitive to boundary irregularity. The three shape descriptors were calculated using a combination of ImageJ and Digital Micrograph 3 software.

3. Results and Discussion

[15] Results for "wet" fuels and "dry" fuels are presented and discussed in the following two sections.

3.1. Wet Fuels (Montana Grass and Tundra Cores)

[16] The SEM images of the particles emitted from the combustion of Montana grass and tundra cores show three basic types of particles: spherical, agglomerates of spherical particles, and crystalline agglomerates. These wet fuels with high fuel moisture content burned with mostly smoldering phase combustion. This resulted in the emission of very spherical and compacted single particles, which are normally formed during the smoldering combustion. Recently, such spherical particles have commonly been called "tar balls" [*Hand et al.*, 2005; *Pósfai et al.*, 2004; *Pósfai et al.*, 2003]. We are not aware of a theory explaining the formation of tar balls; however, a recent study has shown that these spherical particles do not have observable nuclei [*Pósfai et al.*, 2003]. Normally, the particle formation process in flames begins with the creation of condensation nuclei such as polycyclic aromatic hydrocarbons (PAHs) that are consequently pyrolized to form soot [*Turns*, 1996]. However, smoldering combustion is a surface process that begins when most of the volatiles have been expelled from the cellulose fuel [*Chandler*, 1983]. Oxygen diffuses to the surface and reacts exothermally with carbon at temperatures lower than flaming combustion temperatures. Because PAHs tend to form at higher temperatures, the mass fraction of soot produced in smoldering combustion is extremely low, and particle formation may occur around other nuclei. Low-volatility organic compounds (LVOC), released predominantly during the smoldering phase of biomass burning [*Gao et al.*, 2003] often account for a significant part of the condensation nuclei, mainly because of their capability of rapidly condensing [*Eatough et al.*, 2003]. Owing to the polar and hydrophilic nature of many of the LVOC, they grow either by condensation of other semivolatile organic species [*Pankow*, 1994] or by undergoing polymerization with OH radicals in water droplets [*Gao et al.*, 2003]. Tar balls are believed to be formed by a similar mechanism of bimolecular homogeneous nucleation with water vapor and grow by coagulation and condensation [*Pósfai et al.*, 2004]. LVOC released from biomass burning after undergoing polymerization with OH radicals in droplets yield larger molecular weight and less water-soluble species. These changes lead to a reduction of the equilibrium size of the droplet owing to the lowered Raoult effect. As the droplet size decreases, the solution becomes more concentrated and the rate of polymerization enhances, which results in turning the organic polymer largely insoluble in water. Tar balls are believed to be the remaining dry particles.

[17] The composition of the tar balls reported in our study is consistent with what has been reported by previous studies [*Pósfai et al.*, 2003]. However, the carbon background signal from the polycarbonate SEM filter substrate makes it difficult to determine the exact carbon to oxygen ratio of particles. It is not possible to apply any correction factor for the background as it varies from particle to particle. However, some recent studies [*Hand et al.*, 2005; *Pósfai et al.*, 2003] have reported their semiquantitative EDS data analysis and have found it to be fairly consistent with the bulk composition data. Our semiquantitative EDS analysis of particles from Montana grass and tundra core show a very high molar fraction of carbon in most of the particles analyzed, resulting in an average molar ratio of C and O ranging between 5 and 6. This ratio is consistent with those reported by *Pósfai et al.* [2003]. Carbon molar fractions were larger than 75% in over 99% of the particles analyzed. Traces of sulfur and potassium were detected in less than 2% of the particles analyzed, mostly in nonvolatile crystalline agglomerates.

[18] The shape and size of the tar balls observed during this study differ considerably from past studies [*Martins et*

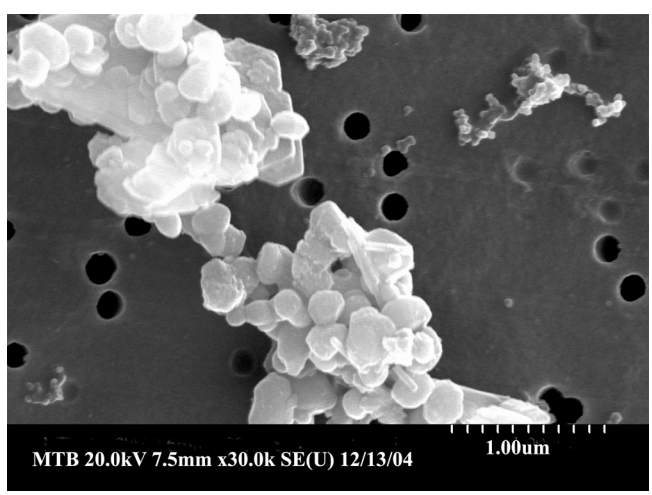

Figure 4. SEM image of irregularly shaped agglomerates built of crystalline palettes.

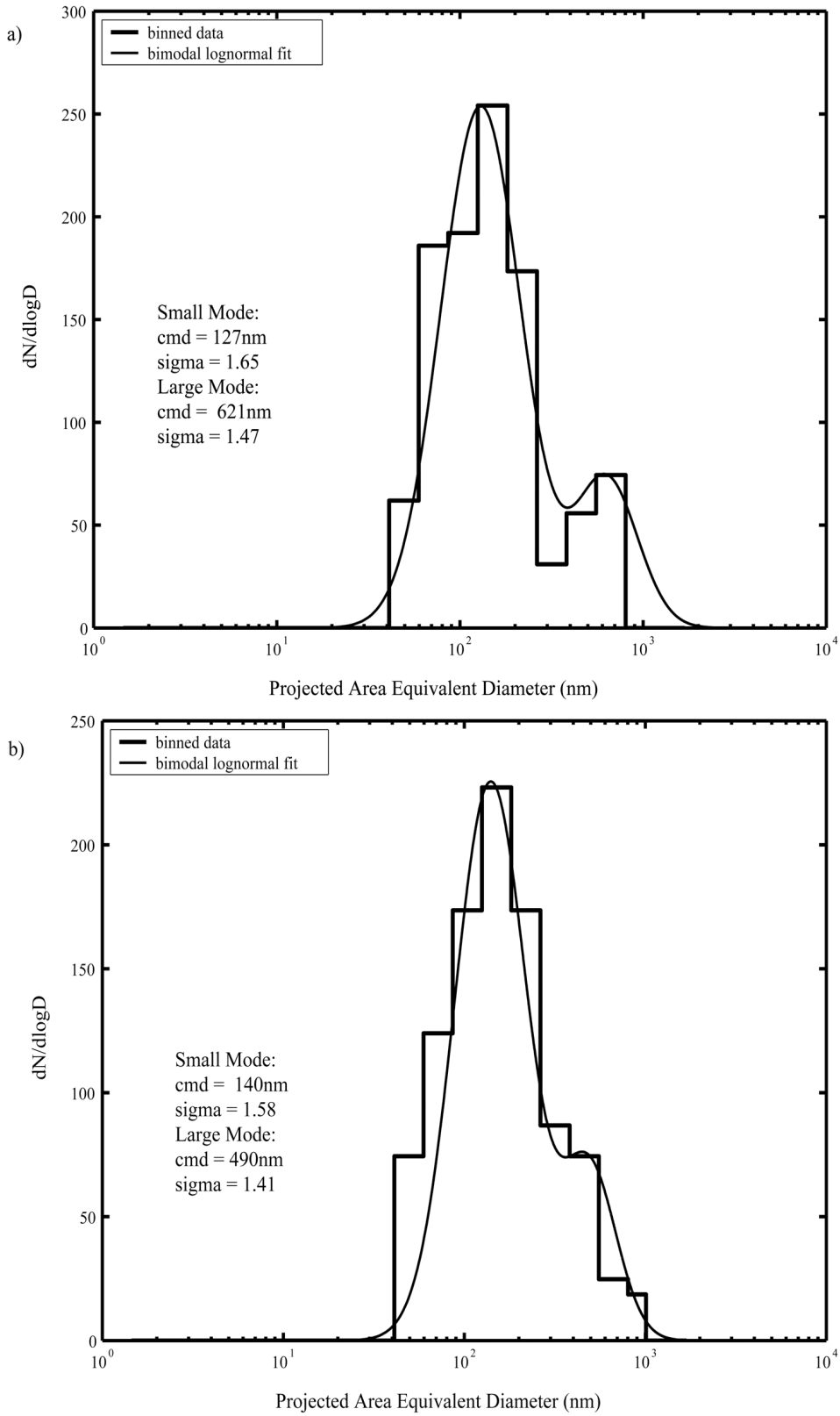

Figure 5. Size distribution of tar balls derived from SEM images of particles emitted from the combustion of (a) tundra cores and (b) Montana grass.

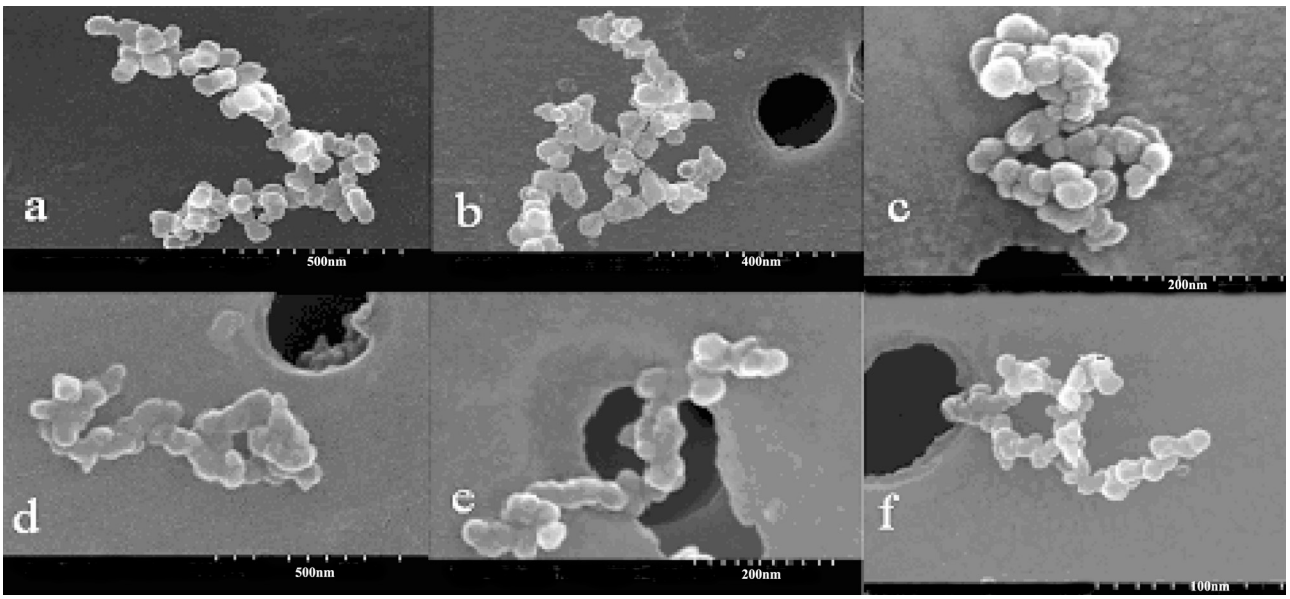

Figure 6. Typical soot particles from the combustion of (a) poplar wood, (b) ponderosa pine wood, (c) ponderosa pine needles, (d) dambo grass, (e) white pine needles, and (f) sagebrush.

al., 1998b; *Pósfai et al.*, 2004; *Pósfai et al.*, 2003]. The tar balls observed in our study are about 2–3 times larger in diameter compared to those reported from Mozambique and Brazil biomass fires (see Figure 2) [*Martins et al.*, 1998b; *Pósfai et al.*, 2004; *Pósfai et al.*, 2003]. More importantly, small and large agglomerates of tar balls were observed, which were not reported in most of the previous studies. Figure 2 shows agglomeration of tar balls into both small and large clusters. Structural defects were also observed in some of the near-spherical tar balls, as is shown in Figure 3. Prolonged atmospheric processing of the tar balls or aging of the particles while fire emissions are drawn through the SEM filter (~10 min), may explain the observed structural defects in some of the tar balls [*Pósfai et al.*, 2004; *Pósfai et al.*, 2003].

[19] The third and the least abundant particle type observed consisted of irregularly shaped agglomerate built of crystalline palettes. On SEM images, these particles are seen as bright features of irregular crystalline agglomerates (see Figure 4). These particles were identified as fly ash, consisting of incombustible material. The lack of any dark areas corresponds to their lack of organic constituents. These particles are insensitive to prolonged exposure to the electron beam and do not lose their bright luster. In addition to carbon and oxygen, the semiquantitative EDS analysis of these particles yielded variable fractions of potassium (K), chlorine (Cl), and sulfur (S).

[20] Size distributions of the tar balls were obtained by measuring their diameters D on the digitized SEM images with the SEM analysis software, where D is defined as the projected area equivalent diameter of a circle or

$$D = 2\sqrt{\frac{A_a}{\pi}}, \tag{3a}$$

where A_a is the projected area of the particle. The diameter D of the particles measured on an SEM image may not be the exact representative of the original diameter of the sphere as seen in the atmosphere, due to flattening of the particles by impaction on the filter substrate and due to loss of semivolatile compounds. Nevertheless, SEM can serve as useful tool for characterizing the size of such aerosol particles.

[21] Number size distributions for tar balls emitted from the combustion of tundra cores and Montana grass are shown in Figures 5a and 5b, respectively. These number size distributions can be represented using bimodal lognormal distributions as shown in Figure 5. The count median diameters (CMD) of the lognormal distributions are 127nm (small mode) and 621 nm (large mode) for tar balls from tundra cores combustion and 140 nm (small mode) and 490 nm (large mode) for particles from Montana grass

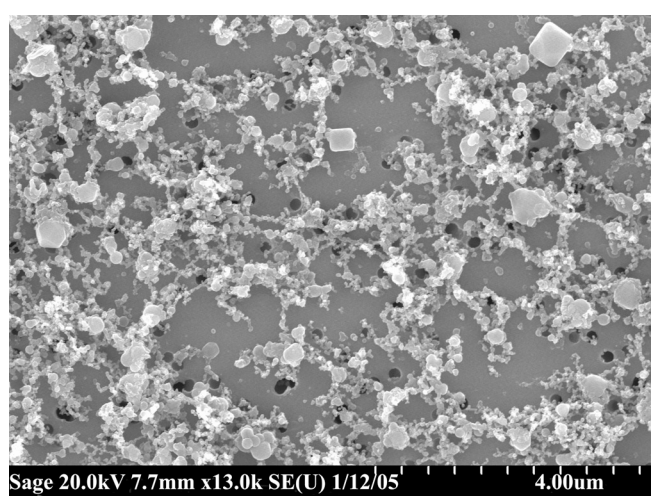

Figure 7. SEM image of particles from the combustion of sagebrush showing the random distribution of spherical and rectangular structures typical for the combustion of the dry fuel samples.

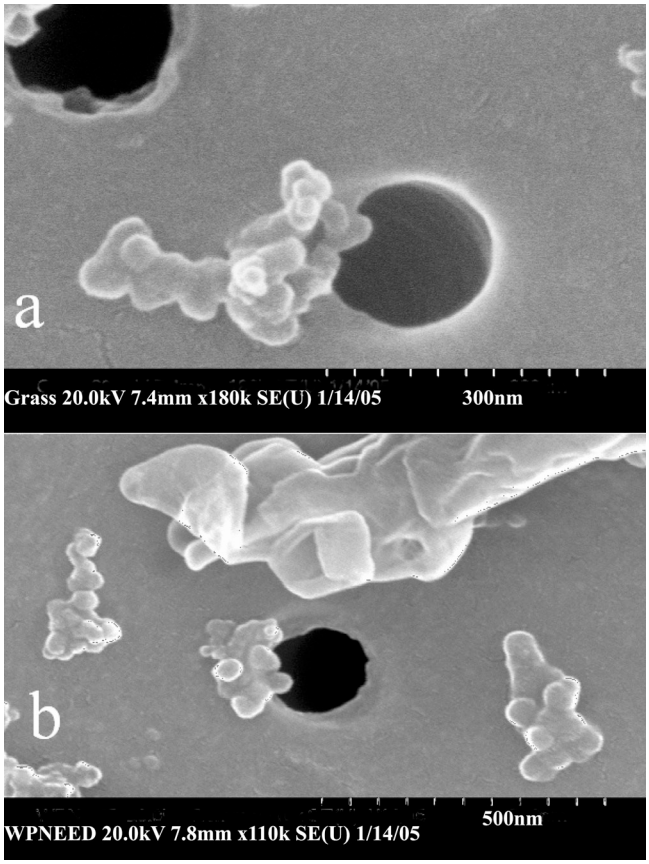

Figure 8. Collapsed soot particles from the combustion of (a) dambo grass and (b) white pine needles indicating coating of organic material on some of the black carbon cores.

combustion. The lower end of the distribution may have been affected by poor collection efficiency of particles smaller than 400 nm in diameter on the SEM filter. These tar ball number size distributions observed in our study show major peaks at large diameters (i.e., around 500 nm) in addition to the peaks at small diameters (i.e., around 130 nm) that are comparable to previous observations of tar balls from biomass fires in Mozambique and Brazil (D $\approx$ 150 nm) and Hungary (D $\approx$ 100 nm). The carbon-to-oxygen molar ratios determined by EDS are comparable for the different sizes observed. The origin of these larger tar balls and the fact that they have not been observed in previous field studies is unclear to us. The size distribution of tar balls observed in our study explains their high albedo, which will be discussed in a future publication.

3.2. Dry Fuels (Sagebrush, Poplar Wood, Ponderosa Pine Wood, Ponderosa Pine Needles, White Pine Needles, and Dambo Grass)

[22] Combustion of these dry fuels occurs with an initial flaming phase followed by a smoldering phase. Therefore combustion yields both fractal aggregates associated with the flaming phase and also smaller spherical particles associated with the smoldering phase.

[23] Particle formation during dry biomass burning is essentially a condensation process. This process begins with the formation of heavy polycyclic aromatic hydrocarbons (PAHs) from ejected fuel gases that condense, forming condensation nuclei allowing for further condensation of other species [*Glassman*, 1996]. Subsequently, these nuclei experience considerable growth and chemical transformations through pyrolysis. Many of these particles may in turn be reduced in size through further oxidation in the interior of the flame zone if temperatures exceed 1100 K [*Glassman*, 1996]. If insufficient oxygen is transported into the flame (extreme oxygen deprived pyrolysis such as in the interior of very large fires) or if the temperature is not high enough to complete oxidation (T < 1100 K), many of these particles may undergo a secondary condensation growth phase and be emitted in the form of smoke. Hence large intense fires of these dry fuels that have very high temperatures and are oxygen limited produce larger soot-based particles with mostly nonspherical chain-like structures [*Martins et al.*, 1998a; *Reid and Hobbs*, 1998].

[24] SEM images of particles generated by the combustion of the dry fuels show that the most predominant particle type is soot (see Figure 6). Soot particles are distinguishable by their unique morphology. They consist of chain aggregates of individual spherules 20–35 nm in diameter [*Pósfai et al.*, 2004; *Pósfai et al.*, 2003]. These spherules are composed of concentrically curved graphite layers similar in structure to an onion [*Hand et al.*, 2005]. The second class of particles were carbonaceous as determined by EDS and were of either spherical or of rectangular structure (Figure 7) and similar to coal fly ash particles [*Hinds*, 1999; *Chen et al.*, 2006]. These particles may be formed during incomplete combustion in the smoldering combustion phase.

[25] Particles from biomass combustion are usually in the accumulation mode [*Reid and Hobbs*, 1998] and have been shown to have three principal components: Particulate organic material (POM; carbon with associated organic matter containing H, N, and O atoms), black carbon (i.e., soot), and trace inorganic species. Usually black carbon

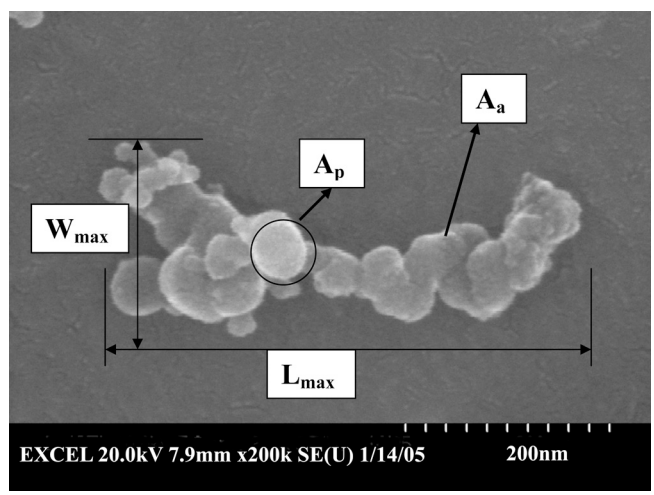

Figure 9. Projected properties of agglomerates measured using image analysis software and routines: projected area A_p of primary particles and projected area A_a, maximum projected length L_{max}, and maximum projected width W_{max} of the agglomerate.

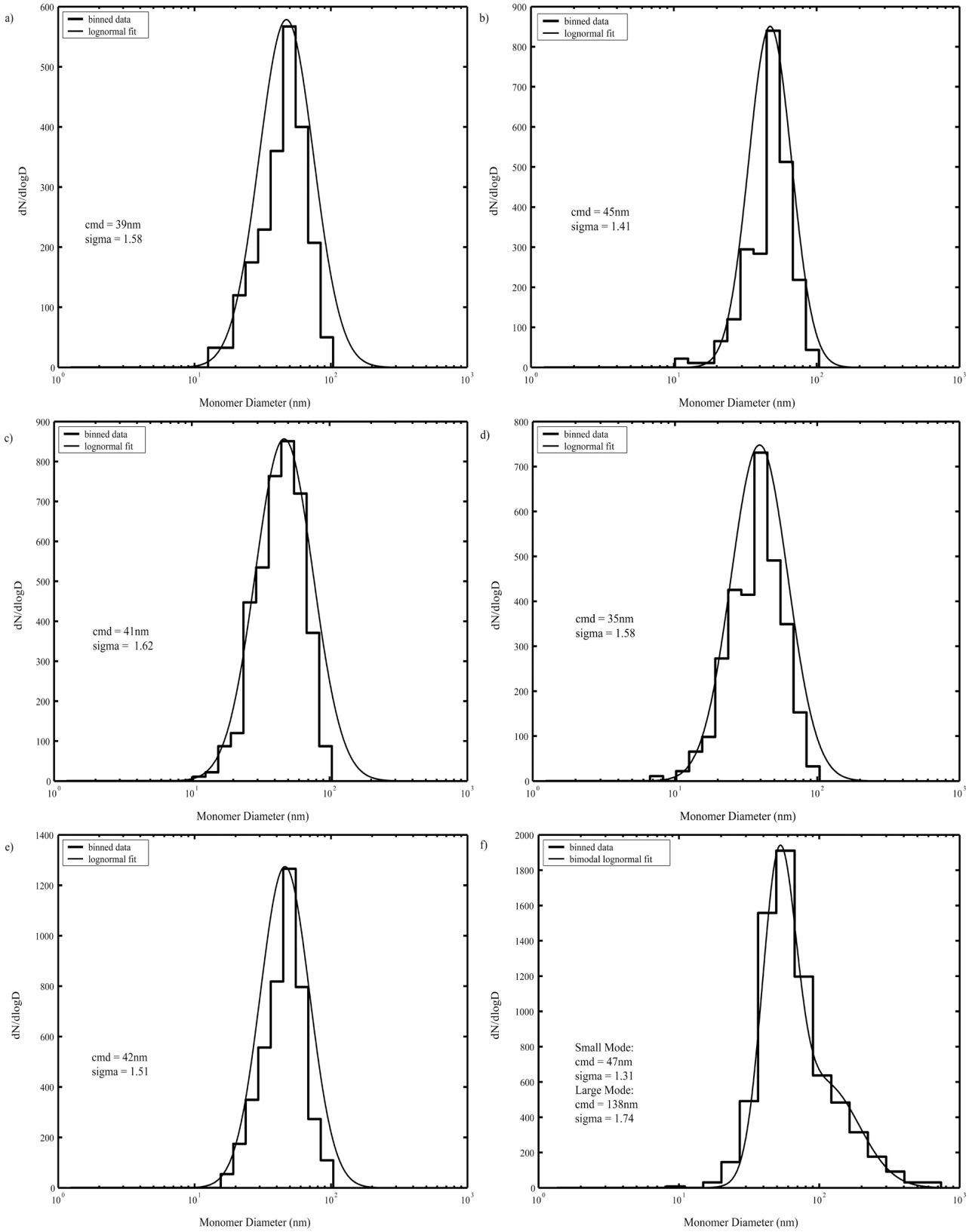

Figure 10. Number size distributions of the monomers from the combustion of (a) dambo grass, (b) white pine needles, (c) poplar wood, (d) ponderosa pine wood, (e) ponderosa pine needles, and (f) sagebrush. Note that the number size distribution of the monomers from the combustion of sagebrush is best represented by a bimodal lognormal distribution.

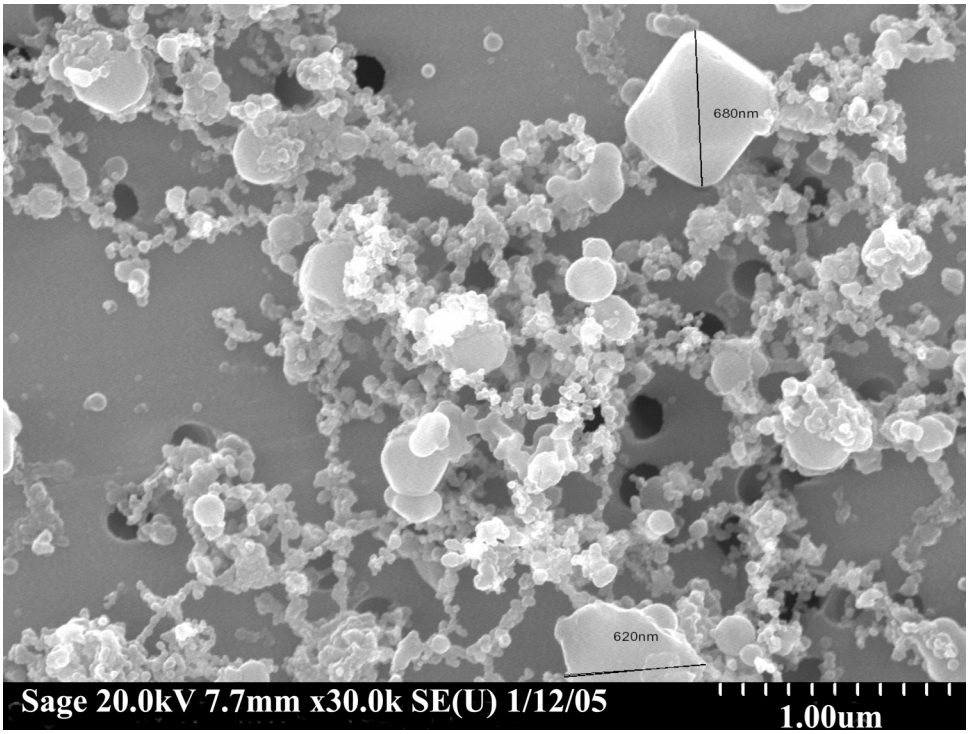

Figure 11. Large irregular shaped particles from the combustion of sagebrush (of maximum two-dimensional length around 600 nm and greater).

(soot) forms fractal chains and does not change its appearance under the SEM upon exposure to the high-voltage electron beam. On the other hand, black carbon cores coated with organic material show up as complex shaped semi-spherical, semiliquid droplets with solid complex cores [*Martins et al.*, 1996; *Martins et al.*, 1998a; *Reid and Hobbs*, 1998]. Collapsed soot particles were also observed for some of the fuels, for example for dambo grass (see Figure 8). The appearance of these particles suggests the presence of an organic coating on some of the black carbon cores.

3.2.1. Two-Dimensional Properties

[26] Primary particle properties characterized with SEM include primary particle diameter d_p and primary particle projected area A_p. Agglomerate properties quantified with SEM include projected area A_a, maximum projected length L_{max}, and maximum projected width W_{max} normal to L_{max}, as illustrated in Figure 9. These measurements are done with the aid of image analysis software (Digital Micrograph 3, Gatan Inc.). To measure the primary particle properties, primary particles clearly distinguishable in agglomerates are selected and their diameters are measured. Figure 10 shows the resulting primary particle size distribution for the six different dry fuels. As can be seen from Figure 10, number size distributions of primary particles emitted from the combustion of almost all of the fuels, with the exception of sagebrush, can be described with a monomodal lognormal number size distribution, with a CMD between 35 and 50 nm, and most primary particles smaller than 100 nm in diameter. The size distribution of primary particles emitted from the combustion of sagebrush can be described with a bimodal lognormal number size distribution, with the CMDs of the two modes being 47 nm and 138 nm. The large mode of this size distribution is largely due to the many large (>100 nm) ash particles that are observed only on the SEM image of particles emitted from sagebrush combustion. In Figure 11 a couple of extraordinarily large ash particles are pointed out and sized.

[27] The projected area of the individual agglomerates was measured through image analysis, and subsequently the projected area equivalent diameters D were calculated. It has been shown previously for TiO_2, Si, and diesel exhaust agglomerates that their projected area equivalent diameter is approximately equal to their mobility diameter [*Park et al.*, 2004; *Rogak et al.*, 1993; *DeCarlo et al.*, 2004] and this relationship may also be valid for other agglomerates such as those from biomass burning. Figure 12 shows the number size distribution of the particles from the combustion of the six dry fuels. The small mode of the distribution essentially constitutes of nonagglomerated single primary particles or very small, chained particles (see Figure 13). For most fuels, the diameter of this small mode peak is comparable to the monomer size with the exception of particles from the combustion of poplar wood where it is nearly twice as large.

[28] The maximum length L_{max} and maximum width W_{max} of agglomerate particles was determined from SEM images. For particles emitted from the combustion of the six different dry fuels used, the maximum length L_{max} scales to the projected area equivalent diameter D with a power law relationship (Figure 14, Table 2) as [*Park et al.*, 2004; *Rogak et al.*, 1993]

$$L_{max} = kD^a, \tag{3b}$$

where a is the exponent characterizing the power law relationship and k is a proportionality constant. As the

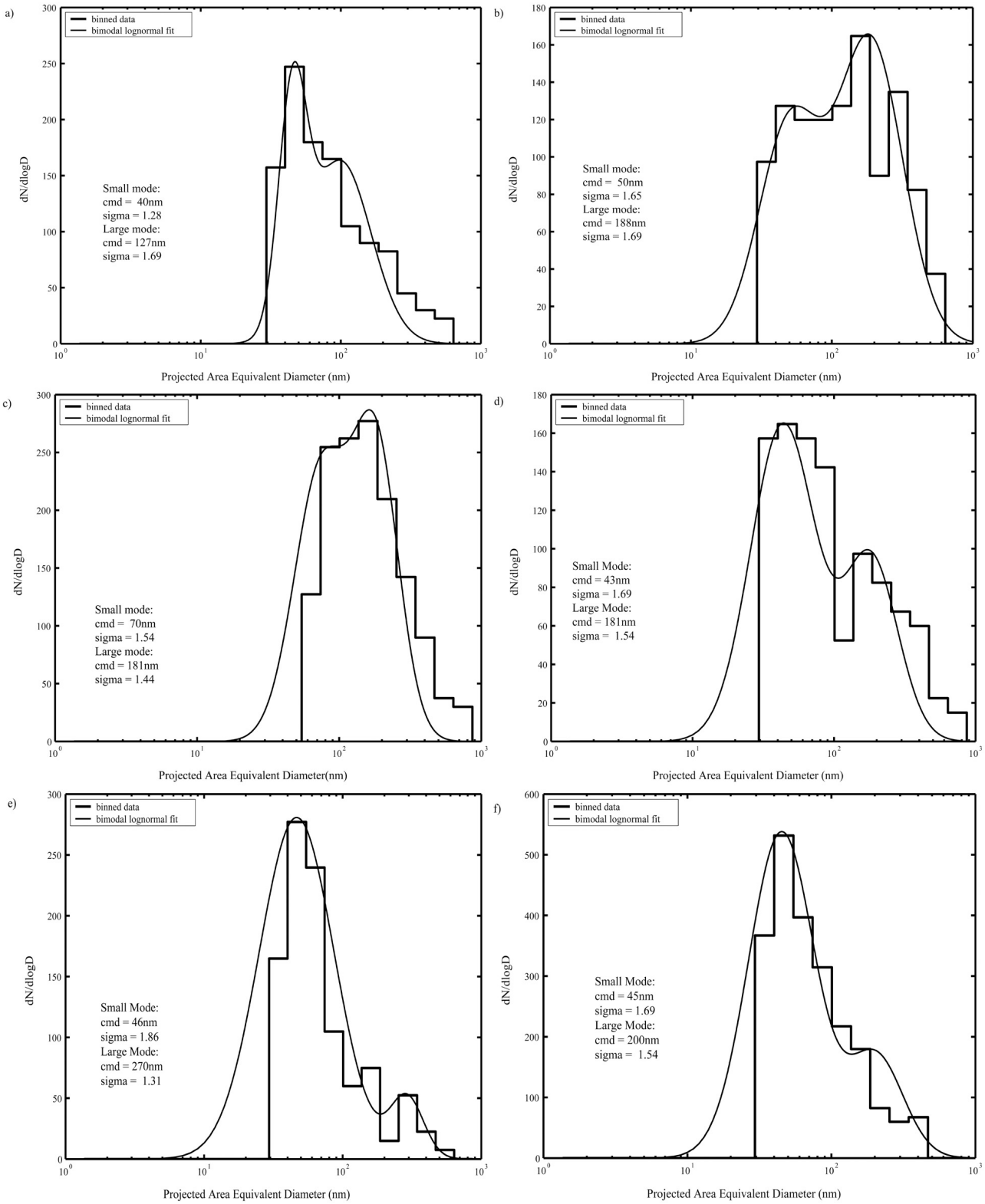

Figure 12. Projected area equivalent diameter *D* distribution for particles from the combustion of (a) dambo grass, (b) white pine needles, (c) poplar wood, (d) ponderosa pine wood, (e) ponderosa pine needles, and (f) sagebrush. The fitted bimodal solid curve shows the expected lognormal number distribution (dN/dlogD).

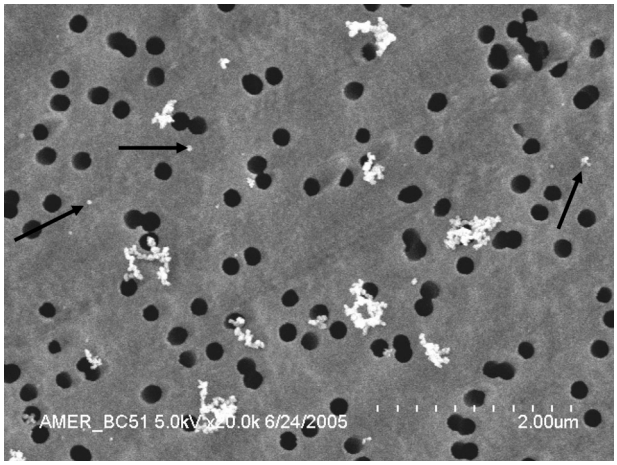

Figure 13. SEM image showing an example of non-agglomerated single primary particles or very small chained particles constituting the small mode of the agglomerate size distribution for the six dry fuels. Note the arrows.

projected area equivalent diameter D can be used as a surrogate for the mobility diameter this power law relationship extends to the mobility diameter. The power law exponent a between the maximum length to the projected area equivalent diameter, the aspect ratio AR, the roundness RN, and the root form factor RFF as determined by image analysis are shown in Table 2 for the different fuels. Note that particles from the combustion of poplar wood have the highest power law exponent a, the lowest proportionality constant k, the lowest aspect ratio AR, the lowest roundness RN, and the lowest root form factor RFF. Particles from the combustion of sagebrush on the other hand have the lowest power law exponent a, the second-highest proportionality constant k, the highest aspect ratio AR, the highest roundness RN, and the second-lowest root form factor RFF.

[29] Figure 15 shows that for our data all three shape descriptors and the proportionality constant k can be parameterized as function of the power law exponent a. The dependence of the root form factor RFF and the aspect ratio AR on the power law exponent a can be described with second-order polynomials, that of the roundness RN and the

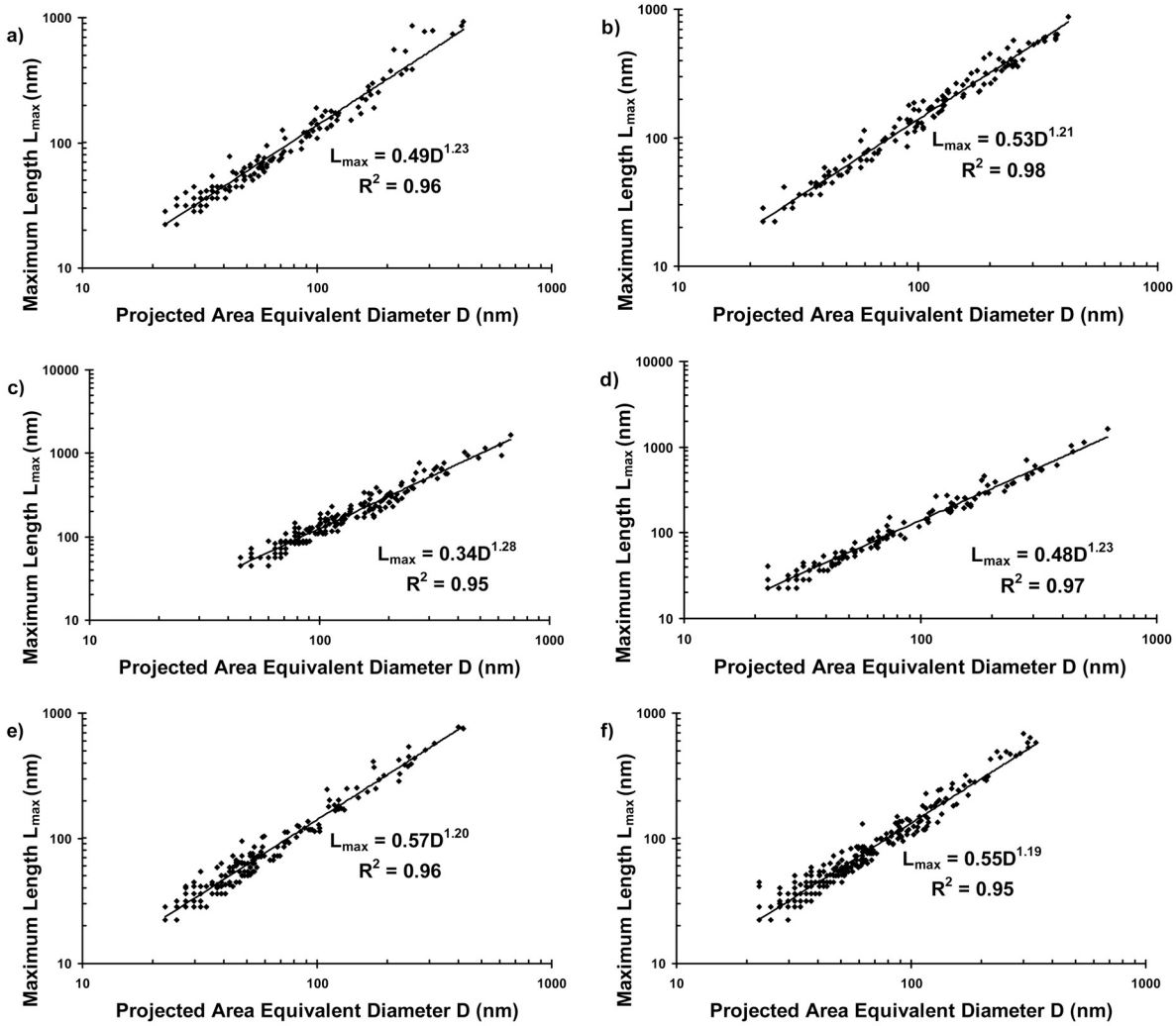

Figure 14. Relationship between the maximum projected length L_{max} and projected area equivalent diameter D for (a) dambo grass, (b) white pine needles, (c) poplar wood, (d) ponderosa pine wood, (e) ponderosa pine needles, and (f) sagebrush.

Table 2. Proportionality Constant k and Power Law Exponent a of the Power Law Relation Between the Maximum Length L_{max} and the Projected Area Diameter D, Aspect Ratio AR, Roundness RN, and the Root Form Factor RFF Values for Particles Emitted From the Combustion of Six Dry Fuels

Fuel	Proportionality Constant k	Power Law Exponent a	Aspect Ratio AR	Roundness RN	Root Form Factor RFF
Sagebrush	0.55	1.19	0.63	0.83	0.86
Poplar Wood	0.34	1.28	0.49	0.73	0.85
Ponderosa Pine Wood	0.48	1.23	0.52	0.78	0.89
Dambo Grass	0.49	1.23	0.52	0.74	0.91
Ponderosa Pine Needles	0.57	1.20	0.58	0.79	0.88
White Pine Needles	0.53	1.21	0.55	0.79	0.89

cubed proportionality constant k^3 by simple linear relationships (Figure 15).

3.2.2. Three-Dimensional Properties

[30] The determination of 3-D fractal dimension of the agglomerates from the 2-D SEM images is possible, provided one has the knowledge of the number of primary particles N and the radius of gyration R_g of the agglomerate. Empirical relationships between 2-D properties and 3-D properties are used to extract 3-D properties from the measured 2-D properties. The number of primary particles can be approximated as [*Oh and Sorensen*, 1997]

$$N = k_a \left(\frac{A_a}{A_p}\right)^{\alpha} \tag{4a}$$

where A_a is the projected area of the agglomerate, A_p is the average projected area of primary particles, k_a is an empirical constant, and α is an empirical exponent. In addition, the estimation of N from A_a/A_p is sensitive to the value of overlap parameter, which is defined for spherical particles as the ratio of the primary particle diameter to the distance between the centers of two touching particles. *Oh and Sorensen* [1997] took the overlapping of primary particles into account and give a graph for the different values of k_a and α to be considered corresponding to different values of overlap parameters ranging between 0 and 2. In our study, the values of α and k_a suggested by *Oh and Sorensen* [1997] corresponding to the different overlap parameters are employed when using equation (4a) to determine the number of primary particles in the agglomerates. A list of average overlap parameters calculated for the different dry fuels are tabulated in Table 3. The radius of gyration R_g can also be extracted from projected properties. Previous studies suggested the maximum projected length L_{max} could be used as a substitute of R_g (i.e., $L_{max}/2R_g$ = constant) [*Brasil et al.*, 1999; *Köylü et al.*, 1995; *Samson et al.*, 1987]. *Oh and Sorensen* [1997] found that $L_{max}/2R_g$ = 1.45, while *Brasil et al.* [1999] determined that $L_{max}/2R_g$ = 1.50. In our study we use the value reported by *Brasil et al.* [1999]. With this approximation, the fractal dimension based on maximum length can be determined as

$$N = k_L \left(\frac{L_{max}}{d_p}\right)^{D_{fl}} \tag{4b}$$

where d_p is the primary particle diameter, k_L is the proportionality constant, and D_{fL} is the fractal dimension when the maximum projected length L_{max} is treated as the characteristic size instead of the radius of gyration R_g. It is important to note that D_{fL} and D_f have identical values and can be used interchangeably. However, equations (1) and (4) have different proportionality constants k_g and k_L that are connected by

$$k_L = k_g \left(\frac{2R_g}{L_{max}}\right)^{D_{fl}} = k_g \left(\frac{2R_g}{L_{max}}\right)^{D_f}. \tag{4c}$$

Figure 16 shows the fractal dimensions D_{fL} of agglomerates from the combustion of different dry wildland fuel calculated with equation (4b). The maximum projected length L_{max} is obtained by direct measurement, while N is determined from equation (2) using values for α and k_a from *Oh and Sorensen* [1997].

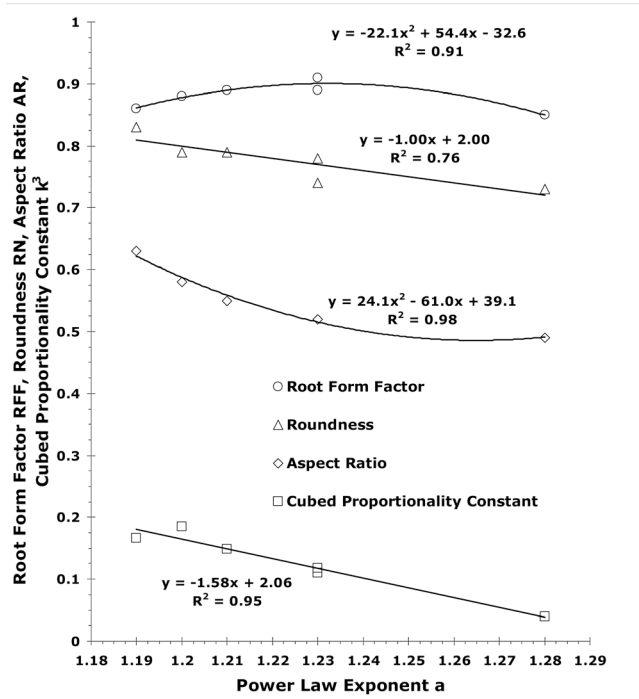

Figure 15. Parameterization of the three shape descriptors and the cubed proportional constant as function of the power law exponent.

Table 3. Three-Dimensional (3-D) Density Fractal Dimension, 2-D Density Fractal Dimension, Textural Fractal Dimension, and Average Overlap Parameter for Particles Emitted by the Combustion of Six Dry Fuels

Fuel	3-D Density Fractal Dimension	2-D Density Fractal Dimension	Textural Fractal Dimension	Overlap Parameter[a]
Sagebrush	1.79	1.68	1.14	1.09 (Point Contact) 1.58
Poplar Wood	1.67	1.69	1.3	1.38
Ponderosa Pine Wood	1.69	1.70	1.11	1.05 (Point Contact)
Dambo Grass	1.76	1.72	1.19	1.36
Ponderosa Pine Needles	1.74	1.73	1.14	1.07 (Point Contact)
White Pine Needles	1.83	1.74	1.13	1.47

[a]For most fuels a single value for the overlap parameter was found, while for sagebrush two values with approximately equal likelihood were found.

[31] Table 3 summarizes the density fractal dimension (D_{fL}) obtained using equation (4b), the 2-D density fractal dimension obtained using nested squares method, and the 2-D textural fractal dimension for the dry fuels. From the table it is evident that the 2-D density fractal dimension obtained using nested squares method clearly underestimates the actual 3-D density fractal dimension of agglomerates. A possible reason for this discrepancy is that the nested squares method does not take into account the partial overlap of primary particles in agglomerates, which is observed frequently in atmospheric particles.

4. Conclusions

[32] The morphology, size, and microstructure of particulate matter emitted from the combustion of eight wild land

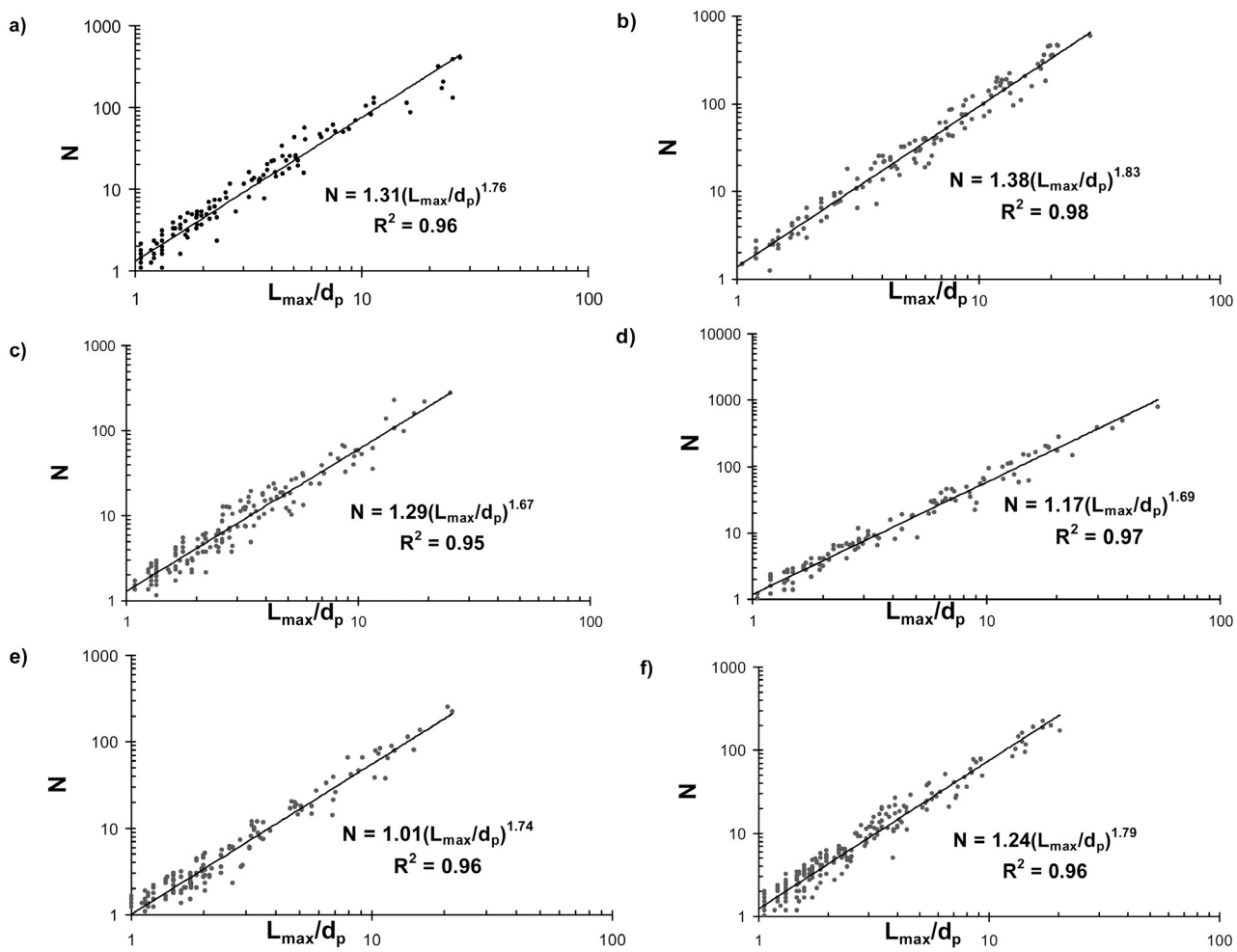

Figure 16. Fractal dimension D_{fL} calculated using equation (4b) for particle agglomerates from the combustion of (a) dambo grass, (b) white pine needles, (c) poplar wood, (d) ponderosa pine wood, (e) ponderosa pine needles, and (f) sagebrush.

fuels (i.e., sagebrush, poplar wood, ponderosa pine wood, ponderosa pine needles, white pine needles, Alaskan tundra cores, African savannah grass, and Montana grass) have been determined. SEM analysis of individual particles from the wet fuels (Alaskan tundra cores and Montana grass) revealed the presence of tar balls. Although tar balls have been observed previously during biomass smoke events, agglomeration of tar balls into small and large clusters had not been reported. The tar balls observed in our study were also larger (diameters ranging to >600 nm) than those reported previously. The shape descriptor roundness, which was used to quantify the circularity of the tar balls, yielded a mean value of 0.96. SEM Analysis of individual particles emitted from the combustion of the dry fuels revealed the presence of mostly sooty chains. These chains, existing as agglomerates of small spherules with primary spherule diameters of 30 to 50 nm, are believed to consist of black carbon and did not show any change in their appearance upon exposure to the electron beam of the SEM. However, the presence of collapsed semiliquid agglomerate chains in some of the samples suggests the presence of organic coatings on some of the black carbon cores. The semiempirical scheme proposed by *Oh and Sorensen* [1997] and *Brasil et al.* [1999] to determine the 3-D fractal dimension of agglomerates from SEM images has been successfully applied for determining the fractal properties of different dry wildland fuels. It was found to be superior to the nested-squares method, which systematically underestimates the mass fractal dimension. The mean values of 3-D density and 2-D textural fractal dimension for the dry fuels range between 1.67 and 1.83 and 1.11 and 1.19, respectively. Three shape descriptors, namely root form factor, roundness, and aspect ratio were used to quantitatively characterize the two-dimensional shape of the particles. A relationship between the three shape descriptors and the proportionality constant k as a function of the power law exponent a was derived. An interesting and challenging future study will be to examine the connection between morphology and optical properties of particles emitted from the combustion of different wildland fuels.

[33] **Acknowledgments.** This work was supported in part by the Joint Venture Agreement 03-JV-11222049-102 between the Desert Research Institute and the USDA Forest Service, Rocky Mountain Research Station, Fire Chemistry Unit, by the Department of Defense, Strategic Environmental Research and Development Program (SERDP) CP-1336, and by the Desert Research Institute. The authors would like to thank Barbara Zielinska and Kihong Park for their insightful suggestions and Mojtaba Ahmadian-Tehrani for his help with the SEM facilities. It is a pleasure to acknowledge the help of Steve Baker, Vladimir Kovalev, Skip Leininger, Jenny Newton, Lynn Rinehart, and Cecily Ryan with the work at the USFS Fire Sciences Laboratory.

References

Ackerman, A. S., O. B. Toon, D. E. Stevens, A. J. Heymsfield, V. Ramanathan, and E. J. Welton (2000), Reduction of tropical cloudiness by soot, *Science*, *288*(5468), 1042–1047.

Brasil, A. M., T. L. Farias, and M. G. Carvalho (1999), A recipe for image characterization of fractal-like aggregates, *J. Aerosol Sci.*, *30*(10), 1379–1389.

Chandler, C. C. (1983), *Fire in Forestry*, John Wiley, Hoboken, N. J.

Chen, L.-W. A., H. Moosmüller, W. P. Arnott, J. C. Chow, J. G. Watson, R. A. Sussot, V. A. Kovalev, and W. M. Hao (2006), Particle emissions from laboratory combustion of wildland fuels: In situ optical and mass measurements, *Geophys. Res. Lett.*, *33*, L04803, doi:10.1029/2005GL024838.

Christian, T. J., B. Kleiss, R. J. Yokelson, R. Holzinger, P. J. Crutzen, W. M. Hao, B. H. Saharjo, and D. E. Ward (2003), Comprehensive laboratory measurements of biomass-burning emissions: 1. Emissions from Indonesian, African, and other fuels, *J. Geophys. Res.*, *108*(D23), 4719, doi:10.1029/2003JD003704.

Colbeck, I., and S. Nyeki (1992), Optical and dynamical investigations of fractal custers, *Sci. Progr.*, *76*(300), 149–166.

DeCarlo, P. F., J. G. Slowik, D. R. Worsnop, P. Davidovits, and J. L. Jimenez (2004), Particle morphology and density characterization by combined mobility and aerodynamic diameter measurements. Part 1: Theory, *Aerosol Sci. Technol.*, *38*, 1185–1205.

Dye, A. L., M. M. Rhead, and C. J. Trier (2000), The quantitative morphology of roadside and background urban aerosol in Plymouth, UK, *Atmos. Environ.*, *34*(19), 3139–3148.

Eatough, D. J., R. W. Long, W. K. Modey, and N. L. Eatough (2003), Semivolatile secondary organic aerosol in urban atmospheres: Meeting a measurement challenge, *Atmos. Environ.*, *37*(9), 1277–1292.

Finlayson-Pitts, B. J., and J. N. Pitts (2000), *Chemistry of the Upper and Lower Atmosphere: Theory, Experiments, and Applications*, 969 pp., Elsevier, New York.

Gao, S., D. A. Hegg, P. V. Hobbs, T. W. Kirchstetter, B. I. Magi, and M. Sadilek (2003), Water-soluble organic components in aerosols associated with savanna fires in southern Africa: Identification, evolution, and distribution, *J. Geophys. Res.*, *108*(D13), 8491, doi:10.1029/2002JD002324.

Glassman, I. (1996), *Combustion*, 631 pp., Elsevier, New York.

Hand, J. L., et al. (2005), Optical, physical, and chemical properties of tar balls observed during the Yosemite Aerosol Characterization Study, *J. Geophys. Res.*, *110*, D21210, doi:10.1029/2004JD005728.

Haywood, J. M., and V. Ramaswamy (1998), Global sensitivity studies of the direct radiative forcing due to anthropogenic sulfate and black carbon aerosol, *J. Geophys. Res.*, *103*(D6), 6043–6058.

Hentschel, M. L., and N. W. Page (2003), Selection of descriptors for particle shape characterization, *Part. Part. Syst. Charact.*, *20*(1), 25–38.

Hinds, W. C. (1999), *Aerosol Technology*, 483 pp., Wiley-Interscience, Hoboken, N. J.

Horvath, H. (1993), Atmospheric light absorption: A review, *Atmos. Environ.*, *27A*(3), 293–317.

Kasischke, E. S., and J. E. Penner (2004), Improving global estimates of atmospheric emissions from biomass burning, *J. Geophys. Res.*, *109*, D14S01, doi:10.1029/2004JD004972.

Katrinak, K. A., P. Rez, P. R. Perkes, and P. R. Buseck (1993), Fractal geometry of carbonaceous aggregates from an urban aerosol, *Environ. Sci. Technol.*, *27*(3), 539–547.

Kaye, B. H. (1989), *A Random Walk Through Fractal Dimensions*, 421 pp., John Wiley, Hoboken, N. J.

Kindratenko, V. V., P. J. M. Van Espen, B. A. Treiger, and R. E. Van Grieken (1994), Fractal-dimensional classification of aerosol particles by computer-controlled scanning electron microscopy, *Environ. Sci. Technol.*, *28*(12), 2197–2202.

Köylü, Ü. Ö., G. M. Faeth, T. L. Farias, and M. G. Carvalho (1995), Fractal and projected structure properties of soot aggregates, *Combust. Flame*, *100*(4), 621–633.

Lohmann, U., and J. Feichter (2001), Can the direct and semidirect aerosol effect compete with the indirect effect on a global scale, *Geophys. Res. Lett.*, *28*(1), 159–161.

Mandelbrot, B. B. (1982), *The Fractal Geometry of Nature*, 460 pp., W. H. Freeman, New York.

Martins, J. V., P. Artaxo, P. V. Hobbs, C. Liousse, H. Cachier, Y. I. Kaufman, and A. Plana-Fattori (1996), Particle size distributions, elemental compositions, carbon measurements, and optical properties of smoke from biomass burning in the Pacific Northwest of the United States, in *Biomass Burning and Global Change*, edited by J. S. Levine, pp. 716–732, MIT Press, Cambridge, Mass.

Martins, J. V., P. Artaxo, C. Liousse, J. S. Reid, P. V. Hobbs, and Y. J. Kaufman (1998a), Effects of black carbon content, particle size, and mixing on light absorption by aerosols from biomass burning in Brazil, *J. Geophys. Res.*, *103*(D24), 32,041–32,050.

Martins, J. V., P. V. Hobbs, R. E. Weiss, and P. Artaxo (1998b), Sphericity and morphology of smoke particles from biomass burning in Brazil, *J. Geophys. Res.*, *103*(D24), 32,051–32,057.

McDonald, R., and P. Biswas (2004), A methodology to establish the morphology of ambient aerosols, *J. Air Waste Manage. Assoc.*, *54*(9), 1069–1078.

National Research Council (1993), *Protecting Visibility in National Parks and Wilderness Areas*, 446 pp., National Academic Press, Washington, D. C.

National Research Council (1996), *A Plan for a Research Program on Aerosol Radiative Forcing and Climate Change*, 161 pp., Natl. Acad. Press, Washington, D. C.

National Research Council Committee on Research Priorities for Airborne Particulate Matter (1998), *Research Priorities for Airborne Particulate Matter*, Natl. Acad. Press, Washington, D. C.

Novakov, T., and J. E. Penner (1993), Large contribution of organic aerosol to cloud-condensation-nuclei concentrations, *Nature*, *365*(6449), 823–826.

Oh, C., and C. M. Sorensen (1997), The effect of overlap between monomers on the determination of fractal cluster morphology, *J. Colloid Interface Sci.*, *193*(1), 17–25.

Pankow, J. F. (1994), An absorption model of gas/particle partitioning of organic compounds in the atmosphere, *Atmos. Environ.*, *28*(2), 185–188.

Park, K., D. Kittelson, and P. McMurry (2004), Structural properties of diesel exhaust particles measured by transmission electron microscopy (TEM): Relationships to particle mass and mobility, *Aerosol Sci. Technol.*, *38*(9), 881–889.

Pósfai, M., R. Simonics, J. Li, P. V. Hobbs, and P. R. Buseck (2003), Individual aerosol particles from biomass burning in southern Africa: 1. Compositions and size distributions of carbonaceous particles, *J. Geophys. Res.*, *108*(D13), 8483, doi:10.1029/2002JD002291.

Pósfai, M., A. Gelencsér, R. Simonics, K. Arató, J. Li, P. V. Hobbs, and P. R. Buseck (2004), Atmospheric tar balls: Particles from biomass and biofuel burning, *J. Geophys. Res.*, *109*, D06213, doi:10.1029/2003JD004169.

Reid, J. S., and P. V. Hobbs (1998), Physical and optical properties of young smoke from individual biomass fires in Brazil, *J. Geophys. Res.*, *103*(D24), 32,013–32,030.

Reid, J. S., T. F. Eck, S. A. Christopher, R. Koppmann, O. Dubovik, D. P. Eleuterio, B. N. Holben, E. A. Reid, and J. Zhang (2005), A review of biomass burning emissions, part III: Intensive physical properties of biomass burning particles, *Atmos. Chem. Phys.*, *5*, 827–849.

Rinehart, L. R., B. Zielinska, H. Moosmüller, W. P. Arnott, J. C. Chow, R. A. Sussot, V. A. Kovalev, and W. M. Hao (2005), Biomass combustion emissions from prescribed burns, wildland fuels, and residential wood combustion, *Environ. Sci. Technol.*, in preparation.

Rogak, S. N., R. C. Flagan, and H. V. Nguyen (1993), The mobility and structure of aerosol agglomerates, *Aerosol Sci. Technol.*, *18*(1), 25–47.

Samson, R. J., G. W. Mulholland, and J. W. Gentry (1987), Structural analysis of soot agglomerates, *Langmuir*, *3*(2), 272–281.

Schult, I., J. Feichter, and W. F. Cooke (1997), Effect of black carbon and sulfate aerosols on the global radiation budget, *J. Geophys. Res.*, *102*(D25), 30,107–30,117.

Seiler, W., and P. J. Crutzen (1980), Estimates of gross and net fluxes of carbon between the biosphere and the atmosphere from biomass burning, *Climatic Change*, *2*, 207–247.

Seinfeld, J. H., and S. N. Pandis (1998), *Atmospheric Chemistry and Physics: From Air Pollution to Climate Change*, 1326 pp., John Wiley, New York.

Sorensen, C. M. (2001), Light scattering by fractal aggregates: A review, *Aerosol Sci. Technol.*, *35*(2), 648–687.

Stachowiak, G. W., and P. Podsiadlo (2001), Characterization and classification of wear particles and surfaces, *Wear*, *249*(3), 194–200.

Turns, S. R. (1996), *An Introduction to Combustion: Concepts and Applications*, 565 pp., McGraw-Hill, New York.

Vedal, S. (1997), Critical review: Ambient particles and health: Lines that divide, *J. Air Waste Manage. Assoc.*, *47*, 551–581.

Watson, J. G. (2002), Critical review: Visibility: Science and regulation, *J. Air Waste Manage. Assoc.*, *52*(6), 626–713.

W. P. Arnott, Department of Physics, University of Nevada, Reno, NV 89557, USA.

R. E. Babbitt, W. M. Hao, E. N. Lincoln, R. A. Susott, and C. E. Wold, USDA Forest Service, Rocky Mountain Research Station, Fire Sciences Laboratory, P. O. Box 8089, Missoula, MT 59807, USA.

R. K. Chakrabarty and H. Moosmüller, Desert Research Institute, Nevada System of Higher Education, 2215 Raggio Parkway, Reno, NV 89512, USA. (rajan.chakrabarty@dri.edu)

M. A. Garro, Department of Chemistry, Harvard University, 12 Oxford Street, Cambridge, MA 02138, USA.

J. Walker, Droplet Measurement Technologies, 5710 Flatiron Parkway, Suite B, Boulder, CO 80301, USA.